Twist Springback and Microstructure Analysis of PEEK Sheets in Ultrasonic-Assisted Thermal Incremental Forming

Juan Liao
Shaocong Zhou
Xin Xue (xin@fzu.edu.cn)
Fuzhou University https://orcid.org/0000-0001-8021-6685

Research Article

Keywords: PEEK, Ultrasonic vibration, Tool trajectory, Twist, Springback, Molecular chain

Posted Date: April 21st, 2022

DOI: https://doi.org/10.21203/rs.3.rs-1561711/v1

Abstract

With a view to reducing the springback and twist of PEEK during the incremental forming process, the ultrasonic vibration is introduced into polymer thermal SPIF. In this study, the effects of temperature and ultrasonic vibration on twist and springback of formed parts are investigated. Several modified tool trajectories are developed, and the influence of tool trajectory on twist and springback are also studied. Finally, the microstructures of PEEK parts are analyzed by XRD. The results show that the increase of temperature is helpful to reduce the twist and springback. The ultrasonic vibration is beneficial to the improvement of geometric accuracy, while the side wall bulge aggravates at 140 ℃ after the ultrasonic vibration is applied. The optimized tool trajectory can effectively eliminate twist and reduce the springback of PEEK parts. The XRD result shows that the ultrasonic vibration is helpful to increase the molecular chain orientation, improve crystallinity and refine crystallite at 60 ℃ and 100 ℃. However, the opposite trend occurs at 140 ℃ due to the disorientation effect of molecular chain.

1. Introduction

Poly-ether-ether-ketone (PEEK) is a kind of special thermoplastic with outstanding properties. PEEK and its composites are increasingly used as customized implants for trauma and cancer or post-infection cranioplasty due to their excellent biocompatibility, stable chemical properties, X-ray penetration and temperature insensitivity. Because of the complexity and particularity of artificial skull in cranioplasty, personalized customization is often required. Nowadays, the main manufacturing method of PEEK skull material is 3D printing and NC milling. Compared with traditional manufacturing technology, 3D printing technology can not only shorten the production cycle and save the production cost, but also achieve high accuracy. However, because the melting temperature of PEEK is as high as 340 ℃, which leads to higher requirements for heating temperature and nozzle design of 3D printer [1]. Traditional CNC milling has high dimensional accuracy. Due to the complex curved surface of actual skull, this method is particularly wasteful of materials and leads to the low utilization rate. Therefore, It is urgent to find a more economical and applicable method to produce artificial PEEK cranial implants.

Recently, some scholars have started to try the single-point incremental forming process (SPIF) to manufacture the cranial implants and prostheses [2–4]. The SPIF process is one of the emerging manufacturing methods because of its flexibility in producing the desired complex shapes with higher formability at low-cost compared to traditional sheet forming methods [5]. Therefore, the SPIF process has very attractive application prospects in small batch production and prototyping in the biomedical sector [6]. According to the characteristics of complex shape, large curvature change and high repair accuracy of actual skull, the SPIF is especially suitable for the manufacture of PEEK cranial implants.

In the study of polymer incremental forming, it is found that the two main defects that have the greatest impact on the forming accuracy of parts are springback and twist [7, 8]. Therefore, it is of great significance to control the twist and springback in the forming process. Ambrogio et al. [9] studied the thermal incremental forming process of thermoplastic and proved that SPIF process is also feasible for

thermoplastic. Yang et al. [10] investigated the effects of heating temperature and step depth on the forming force, geometric accuracy and twist of PEEK SPIF parts. In recent years, some scholars have introduced ultrasonic vibration into the field of plastic forming of metals. It is found that applying ultrasonic vibration with a certain amplitude and frequency can improve the friction conditions [11], reduce the forming force [12], decrease the amount of springback [13], and improve the geometric accuracy and forming quality of forming parts. However, the effect of ultrasonic vibration on twist and springback of polymer SPIF has not been reported.

PEEK is a semi-crystalline polymer. Its microstructure is divided into crystalline and amorphous region, which is mainly composed of stacked lamellar structure and amorphous molecular chains entangled between lamellae. The co-existence of crystalline and amorphous region makes the polymer both rigid and ductile. However, the structural evolution caused by the forming process will change the mechanical properties of polymers, so it is very important to explore the structural evolution during the deformation process. Davarpanah et al. [14] noticed the deformation-induced chain reorientation in the thermoplastic polymer SPIF process. Hata et al. [15] evaluated the influence of molecular chain deformation behavior on mechanical properties of PLLA and found that the elongation and angle change of molecular chain had a large influence on stress. Wei et al. [16] analyzed the tensile properties and structure of polymer after ISF and found that with the increase of strain, the crystallinity of the material decreased. In terms of metal SPIF, Lu et al. [17] found that the application of low-frequency vibration in SPIF at room temperature could significantly refine the grain of magnesium alloy (AZ31) sheet. Sakhtemanian et al. [18] reported that ultrasonic vibration reduced the friction coefficient and refined grains of St/Ti bimetal plate in the SPIF. Nonetheless, the effect of ultrasonic vibration on the microstructure of polymer SPIF process is still remain unknown.

In this work, ultrasonic vibration is introduced into polymer thermal SPIF process. By taking the typical pyramid frustum as example, the effects of temperature and amplitude on the springback and twist of PEEK parts are analyzed. Then, the tool trajectory is optimized to study its effect on twist and springback reduction. Lastly, the effects of temperature and ultrasonic vibration on the microstructure are also analyzed by XRD.

2. Experiment Details

2.1 Experiment setup

The experimental platform of this study is built on a 3-axis Computer Numerical Control (CNC) milling machine, which equipped with heating workspace and ultrasonic vibration device. As shown in Fig. 1(a), the experimental setup is mainly composed of four parts: working platform, electric heating system, temperature monitoring and control system, and ultrasonic vibration device. The working platform is fixed on the CNC milling machine and consists of supporting structure, blank holder plate and quick fixture (Fig. 1(b)). It is mainly used for supporting and clamping the polymer sheet. The electric heating system is mainly composed of four carbon fiber electric heating tubes. The electric heating tubes are connected

with the PID temperature controller, and evenly arranged inside the workspace to heat the sheet through heat radiation. The temperature monitoring and control system is mainly composed of infrared thermometer and IR camera. The infrared thermometer is connected with the PID temperature controller, and feedback signal to the PID controller to control the sheet forming temperature. The IR camera is used to record the temperature distribution during the SPIF process (see Ref. Liao et al. [19] for complete details).

The ultrasonic vibration device primarily consists of ultrasonic generator, transducer, amplitude amplifier, forming tool head and cooling water circulation device. The ultrasonic generator generates high-frequency current signal, and the electrical energy is converted into mechanical vibration through the transducer. The vibration is transmitted to the forming tool head through an amplitude amplifier. The frequency of ultrasonic vibration is 20 kHz and the amplitude is adjustable in the range of 0 ~ 20 μm. The cooling water circulation device is used to cool the transducer during the forming process to prevent the transducer from being damaged by excessive temperature.

2.2 Material and experiments

In this work, PEEK sheets with a thickness of 3 mm are employed. The PEEK sheet is cut into rectangular sheets with a size of 200×200 mm by using a shearing machine. In order to study the thermal mechanical properties of PEEK, the Shimadzu AG-Xplus universal testing machine with a thermostatic chamber is used for the tensile test. The tensile specimens refer to ISO 527 standard. The experimental temperatures are set as 60 ℃, 100 ℃ and 140 ℃ respectively, and the tensile speed is 50 mm/min. To ensure temperature uniformity of the specimen, the temperature of the thermostatic chamber was maintained for 20–30 minutes after reaching the target temperature. The results are presented in Fig. 2(a). It can be observed that with the increase of temperature, the elasticity modulus E and yield stresss σ_Y of the material show a decreasing trend, and the plasticity of the material is improved obviously.

The glass transition temperature (T_g) of PEEK is 143 ℃. To prevent thermal deformation caused by excessive temperature, the polymer sheets are heated to a temperature slightly lower than Tg. Then the sheets are deformed by UV-assisted thermal SPIF under different amplitudes. The target shape of the forming part is shown in Fig. 2(b). As shown in Fig. 2(c), the unidirectional contour trajectory (UCT) is adopted in the experiment. The diameter of ultrasonic vibration tool head is 10 mm. The step depth is 0.5 mm, and the feed speed is 1000 mm/min.

First, a series of experiments at different temperatures (60 ℃, 100 ℃, and 140 ℃) and ultrasonic amplitudes (0 μm, 10 μm, and 20 μm) are conducted to study the effects of temperature and ultrasonic vibration on the twist and springback in PEEK thermal SPIF process. Secondly, four different modified tool trajectories are developed based on the original trajectory (UCT). Ultrasonic assisted thermal SPIF experiments with different trajectories are also conducted to explore the influence of different trajectories on the twist and springback of PEEK parts. The molybdenum disulfide high temperature grease is used for lubrication in the forming process.

2.3 Measurement and evaluation methods

Twist angle φ is one of the key factors to evaluate the geometric accuracy of polymer. Because the tool trajectory is unidirectional, the material flows and accumulates along the path, resulting in twisting [20]. In order to quantitatively measure the twisting caused by the SPIF process, a cross line is marked on the polymer sheet before forming. The twist angle of the part can be obtained by measuring the deflection angle of the cross line after forming, as shown in Fig. 3(a).

Springback is a common defect in thermal SPIF process due to the sheet bending effect. In order to comprehensively analyze the springback of parts after forming, the springback is mainly divided into three regions for quantitative measurement, as shown in Fig. 3(b): the springback angle θ_1, the springback angle θ_2 and the curl radius ρ of the side wall. The three-dimensional (3D) surface scanning device is used to obtain the cross section contour curve of the forming part. Finally, θ_1, θ_2 and ρ were measured by CAD.

X-ray diffraction (XRD) technology is a method to obtain the internal structure of materials by analyzing the diffraction patterns. In this work, XRD is used to analyze the molecular chain orientation, crystallinity and crystallite size of polymer. During the SPIF process, the ultrasonic vibration tool head mainly acts on the side wall of the part, so the material at side wall is selected as the observation object. For the XRD analysis, a rectangular sample is taken from the wall of the square pyramid parts, as shown in Fig. 4.

3. Results And Discussion

3.1 Effects of temperature and amplitude on twist and springback

The deformed parts at different temperatures and ultrasonic amplitudes are compared in the Fig. 5. It can be observed that the formed parts have different degrees of twist under the unidirectional trajectory. The twist angle φ and springback angle θ_1, θ_2, sidewall curl ρ of the formed parts are summarized in Table 1.

Table 1
The values of twist angle φ and θ_1, θ_2, ρ.

T/(℃)	A/(μm)	Twist angle φ/(°)	θ_1/(°)	θ_2/(°)	ρ/(mm)
60	0	8.8	149.7	132.8	86.8
	10	8.0	148.9	133.8	107.2
	20	7.2	148.5	133.8	105.5
100	0	9.7	144.8	131.8	83.2
	10	9.1	144.3	132.5	93.4
	20	8.1	142.6	132.3	92.9
140	0	6.2	140.2	136.0	76.2
	10	5.4	138.1	135.3	52.0
	20	4.8	137.3	135.1	63.3

3.1.1 Twist

As shown in Fig. 6, with the increase of forming temperature, the twist angle φ of PEEK parts increases slightly and then decreases significantly near T_g. When the temperature begins to rise, the contact friction coefficient between sheets and tool head increases. The increase of tangential force aggravates the twist. However, when the temperature is close to T_g, the softening effect of polymer is more obvious. At this time, the softening effect of material exceeds the effect of increasing friction coefficient. The polymer softening significantly reduces the forming force, so as to reduce the tangent force driven by tool head along the tool trajectory, thus reducing the twist angle. By increasing the temperature, the reduction rate of φ reaches 33%.

In order to verify the increase of temperature reduces the tangential force, the scratches on the inner surface of parts are observed. Figure 7 shows the scratches on the inner surface of the formed part at different temperatures caused by the interaction of tool head. Figure 7 (b,c) shows that there are sharp scratches on the inner surface of PEEK parts at the forming temperatures of 60 ℃ and 100 ℃, and the scratches are obviously alleviated at 140 ℃ (Fig. 7 (d)). It also indicates that the tangential force between the tool head and the sheet is reduced with the increase of temperature.

According to the comparative experimental results at different amplitudes as shown in Fig. 6, the application of ultrasonic vibration can reduce the twist angle φ of polymer, and the twist angle decreases gradually with the increase of amplitude. The maximum reduction rate of φ reaches 23% under the ultrasonic vibration effect. This phenomenon may be due to the periodic discontinuous contact between the tool head and part surface caused by ultrasonic vibration. It reduces the friction and tangential force, resulting in the reduction of twist angle.

3.1.2 Springback

Springback is another major problem of low geometric accuracy in polymer SPIF. The springback mainly includes the continuous local springback around the tool and the global springback after the release of the tool and fixture. The spingback of parts are mainly reflected in the blank holder area, bottom area and side wall. In order to more intuitively compare the effects of ultrasonic vibration and amplitude on springback, the θ_1, θ_2 and ρ values are summarized and compared in Fig. 8.

Figure 8(a) shows that the springback angle θ_1 and θ_2 are closer to the target value with the increase of temperature, indicating that the increase of temperature can improve the geometric accuracy of the blank holder area and bottom area of parts. Similar trends are observed in samples with different amplitudes, but the effect is not as significant as temperature. It means that ultrasonic vibration have less effect on the springback angle of blank holder area and bottom area. Under the effect of temperature combined with ultrasonic vibration, the errors of θ_1 and θ_2 decrease from 14.7° and 3.2° to 2.3° and 0.1°, respectively.

As can be seen from Fig. 8(b), the curl radius ρ of sidewall tends to decrease slightly as the temperature increases. The smaller the curl radius, the more severe the sidewall bulge. It means that the higher temperature reduces the geometric accuracy of the sidewall. Comparing the samples under different amplitudes, it can be found that the effect of ultrasonic vibration on sidewall bulge is greater than that of temperature. Meanwhile, it indicates that the ultrasonic vibration can inhibit the bulge of side wall at 60 ℃ and 100 ℃, while it aggravates the bulge at 140 ℃. The reason for this phenomenon will be explained later.

In order to further explore the influence of ultrasonic vibration on the forming uniformity of part, the thickness of the formed part is measured by thickness gauge at intervals and the thickness distribution diagram is plotted in Fig. 9. As shown in Fig. 9 (a-c), it can be found that the increase of temperature improves the uniformity of part thickness distribution. Moreover, Fig. 9(d) shows that when the temperature increases from 60 ℃ to 140 ℃, the maximum thinning rate of formed part also shows a decreasing trend.

Comparing the samples at the same temperature in Fig. 9, it can be found that the increase of amplitude also improves the uniformity of part thickness distribution. The reduction rate of maximum thinning rate is 3.7%, 2.0% and 4.0% for the part at 60°C, 100°C, and 140°C after applying ultrasonic vibration of 20 μm. These results indicate that increasing temperature and amplitude can improve the forming uniformity of PEEK parts. The increase of forming uniformity is beneficial to reduce the accumulation of residual stress during SPIF process, thus reducing the springback.

These results show that the increase of temperature and the application of vibration can inhibit the twist and springback of SPIF parts. Moreover, the parts have less twist and springback at 140 ℃ and 20 μm amplitude.

3.2 Effect of modified tool trajectory on twist and springback

Although the previous results indicate that appropriate temperature and ultrasonic vibration have an inhibitory effect on the twist and springback of PEEK parts, there are still a certain degrees of twist and springback. Therefore, in order to further reduce the twist and springback of PEEK parts, the modified tool trajectories are developed.

As shown in Fig. 10(a,b), equidistance spiral trajectory (EST) and non-equidistance spiral trajectory (NEST) are generated. EST is the spiral trajectory with a constant step depth (0.5 mm). NEST is the spiral trajectory with increasing step depth from 0.25 mm to 1.5 mm. Figure 10(c,d) shows the mixed contour trajectory with 0.5 mm step depth (MCT-0.5) and the mixed contour trajectory with 1.5 mm step depth (MCT-1.5). The spiral and contour trajectories are designed to investigate the effect of different loading methods on twist and springback. The different step depths are used to compare the effects of step depths on twist and springback. Based on the previous experience, the forming experiments with different trajectories are carried out at 140 ℃ and 20 μm amplitude.

3.2.1 Twist

Figure 11 shows that under the action of the UCT, the part twist 4.8° along the loading direction. Moreover, the parts deformed with the EST and NEST shows larger twist deformation, i.e. 6.8° and 8°. It means that parts deformed by unidirectional loading with either contour or spiral trajectory shows serious twist deformation. However, under the action of MCT (both MCT-0.5 and MCT-1.5), the twist of PEEK parts is almost eliminated. This indicates that the twist of PEEK parts can be effectively suppressed by the alternant loading trajectory of clockwise and counterclockwise. Meanwhile, MCT with different step depths shows similar effect on twist reduction.

3.2.2 Springback

For a more intuitive comparison of the effect of trajectory on springback, the section shape and the forming height of the PEEK parts are measured. Higher forming height represents less springback in height direction. Less error between actual and ideal geometry shows better geometric accuracy. Figure 12(a) compares the section shapes of the formed parts under different trajectories. It can be seen that MCT-0.5 is closest to target height, while NEST is furthest from the target height. As shown in Fig. 12(b), the forming heights of MCT-0.5 and NEST are 38.5 mm and 35.2 mm (target height is 40 mm), and the minimum and maximum errors are 1.5 mm and 4.8 mm respectively. This indicates that the part deformed under MCT-0.5 has the best geometric accuracy. Under the action of MCT-0.5, the forming height is increased by 9.4% and the error is reduced to 1.5 mm compared with NEST.

Figure 13 (a, b) also shows that the springback angles θ_1, θ_2 are closer to the target value at UCT and MCT-0.5. And under the action of MCT-0.5, PEEK parts have the maximum curl radius ρ. However, EST

and NEST show poor geometric accuracy. These also indicate that PEEK parts of MCT-0.5 have the least springback compared to the other trajectories.

These results illustrate that MCT has an obvious inhibitory effect on twist and springback due to the bidiretional loading, and it has the least springback at smaller step depth (MCT-0.5). However, the smaller the step depth, the longer the forming time and the lower the processing efficiency will be. Therefore, considering both processing efficiency and geometric accuracy, MCT with appropriate step depth should be considered in PEEK SPIF.

3.3 Microstructure analysis

In the forming process of semi-crystalline polymers, a series of changes occur, such as reorientation of molecular chain, crystal breakage and microcrystal rearrangement. In addition, the mechanical properties of semi-crystalline polymers are closely related to the orientation of molecular chains, crystallinity and crystal structure [21, 22]. Therefore, it is of great significance to investigate the microstructure evolution of semi-crystalline polymers during the SPIF process. Figure 14 plots the integrated intensity versus 2θ curves of the unformed PEEK. It is concluded that PEEK has a semi-crystalline structure, evidenced by the clear high intensity peak and wide low intensity signal. The former corresponds to the crystallized part and the latter corresponds to the amorphous part. The XRD pattern shows peaks of the diffraction planes (110), (111), (200) and (211) of the PEEK in around 18.6°, 20.6°, 23.2° and 28.9°, respectively. In addition, the crystallinity of the unformed material and the crystallite size of each diffraction plane are also measured and shown in Fig. 14.

3.3.1 Molecular chain orientation

The entanglement of molecular chains is one of the important characteristics of polymer microstructure. During polymer processing, the material shows high deformation resistance due to the entanglement of molecular chains, which will cause considerable difficulties in forming. The mechanical properties of polymers depend significantly on orientation of molecular chains [23, 24]. Greater degree of orientation enables molecular chains to slide past each other easily during deformation, resulting in lesser elastic stiffness and better plastic deformation ability [14].

Figure 15 plots the XRD patterns of PEEK parts at different temperatures. If the molecular chain of the polymer is preferably oriented in one direction, a greater intensity can be seen in the diffraction peak [25]. At the major peaks (2θ = 18.6°, 20.6°, 23.2°), the intensities are generally higher for the part under 140 ℃ as compared to 60 ℃ and 100 ℃. This indicates greater chain orientation in the part of 140 ℃ along these directions. When the forming temperature reaches 140 ℃, the higher temperature will enhance the activity of molecular chain and easily de-entangle the molecular chain. Therefore, the forming temperature close to T_g will increase the degree of orientation, so as to improve the plastic deformation ability of the material and reduce the ability to resist deformation. This is also the reason why the springback decreases when the temperature increases in the polymer SPIF process.

As can be seen from Fig. 16(a,b), the intensities of the major peaks of the PEEK formed parts under 60 ℃ and 100 ℃ increase with the application of ultrasonic vibration and the increase of amplitude. It means greater orientation of parts at 60 ℃ and 100 ℃ due to the application of ultrasonic vibration. The high frequency ultrasonic vibration will weaken the intermolecular force of polymer, enhance the activity of chain segments, and promote the untangling of molecular chain under the action of ultrasonic vibration. It is likely that when the forming temperature is lower than T_g, the application of ultrasonic vibration can reduce the deformation resistance of the material, increase the fluidity of the polymer, and improve the processability at the molecular level.

Figure 16(c) shows that the intensities of major peaks in the parts under 140 ℃ decrease to a certain extent after the ultrasonic vibration is applied. Yang et al. [26] noticed that when the ultrasonic vibration reached a certain extent, slip systems of the aluminum sheet influenced each other and caused a hindrance to dislocation motion. Hence, the intensity of the external force was further increased to circumvent obstacles between dislocations, and it resulted in a hardening effect of ultrasonic vibration. For semi-crystalline polymer sheets, as the forming temperature approaches T_g, the higher temperature makes the molecular chain more active, and the chain segments have been tightly arranged and ordered. However, the application of ultrasonic vibration at this time may not enhance the ordered arrangement, but may break the existing tight structure. Due to the lower orientation of the molecular chain, the "hardening effect" of the polymer occurs, which increases the deformation resistance and results in the increase of springback. This is also the reason why the side wall bulge of PEEK part increases when ultrasonic vibration is applied at 140 ℃.

3.3.2 Crystallinity and crystallite size

For further analysis, the crystallite size is estimated by Scherrer Equation [27], as shown in Eq. (1):

$$D=\frac{K\lambda}{\beta\cos\theta}$$

1

Where K is a constant, λ is the wavelength of radiations, θ is the diffraction angle, β is the full width at half maxima of the diffraction peak. The crystallinity of each sample is defined by the ratio of crystalline and amorphous diffraction peaks, and it is shown in Fig. 17(a). The crystallite size of the main crystalline diffraction plane (110) is estimated by Eq. (1) and then plotted in Fig. 17(b).

It can be inferred from Fig. 17(a,b) that the crystallinity of the formed parts are lower than that of the unformed part due to crystal breakage caused by uneven deformation at 60 ℃ and 100 ℃, and the crystallite size of the formed parts are also significantly smaller than that of the unformed part. After the ultrasonic vibration is applied, the crystallinity of the samples at 60 ℃ and 100 ℃ recover to some extent, and the crystallite size further decrease. Studies [28, 29] reported that the chain orientation influences the crystallization kinetics in polymer crystallization. Therefore, the orientation effect of molecular chain caused by ultrasonic vibration at 60 ℃ and 100 ℃ may induce the crystallization and

nucleation of PEEK, so as to improve the crystallinity and reduce the crystallite size. The crystallite refinement at 60 ℃ and 100 ℃ may improve the plasticity and processability of material, reduce the stress accumulation during the SPIF process, thus reduce the springback. However, the molecular chain disorientation effect of parts at 140 ℃ after the ultrasonic vibration is applied, results in the opposite trend (both microstructure and mechanical properties).

The results of XRD show that the appropriate forming temperature can improve the orientation of molecular chains. Moreover, the application of ultrasonic vibration at 60 ℃ and 100 ℃ can further increase the molecular chain orientation, improve the crystallinity and refine the crystallite. This is beneficial to reduce the deformation resistance and springback in the SPIF process. However, the application of ultrasonic vibration at 140 ℃ cannot improve the tight arrangement of the molecular chain, but will reduce the degree of orientation.

4. Conclusions

In the current study, ultrasonic-assisted thermal SPIF experiments of PEEK sheets are performed. The twist and springback of parts at different temperature and amplitude are studied. The effect of tool trajectory on twist and springback of formed parts are also investigated. Finally, the evolution of molecular chain, crystallinity and crystallite size in SPIF process are analyzed by XRD. The obtained results can be summarized as follows:

(1) With the increase of forming temperature, the twist angle of formed parts increases slightly and then decreases significantly. The application of ultrasonic vibration and appropriate amplitude are helpful to reduce the twist.

(2) As the temperature rises, the springback of most areas of the part decreases. The ultrasonic vibration helps to further reduce the springback in the blank holder area and the bottom area. The application of ultrasonic vibration at 60 ℃ and 100 ℃ alleviates the side wall bulge of the part. However, the side wall bulge aggravates after the ultrasonic vibration is applied at 140 ℃.

(3) Under the action of modified tool trajectory, twist and springback are further reduced. With the mixed contour trajectory (MCT), the twist of PEEK parts are almost eliminated, and with the MCT at appropriate step depth, the springback can be significantly reduced and the geometric accuracy of PEEK parts are improved.

(4) When the forming temperature reaches 140 ℃, the molecular chain has a greater degree of orientation. The ultrasonic vibration is helpful to increase the molecular chain orientation and reduce the deformation resistance at 60 ℃ and 100 ℃. On the contrary, the application of ultrasonic vibration at 140 ℃ will lead to the disorientation of molecular chains.

Declarations

Acknowledgements The authors would like to express many thanks to Ms. Lisha Zhang and Mr. Xiangshou Zeng for the help of some experimental work and suggestions.

Authors' contributions All authors contributed equally to the generation and analysis of experimental data, and the development of the manuscript.

Funding This work received the financial support by the National Natural Science Foundation of China (No. 51805087).

Code availability Not applicable

Availability of data and material This study is based only on data obtained using the methods described in this paper

Ethics approval All authors declare that his article does not have any academic ethics issues and strictly follows the journal submission rules.

Consent to participate All authors agree to participated in this research work.

Consent for publication All authors agree to publish this work.

Conflict of interest The authors declare no competing interests.

References

1. Wang P, Zou B, Xiao HC, Ding SL, Huang CZ (2019) Effects of printing parameters of fused deposition modeling on mechanical properties, surface quality, and microstructure of PEEK. J Mater Process Technol 271:62–74. DOI: 10.1016/j.jmatprotec.2019.03.016
2. Oleksik V, Pascu A, Deac C, Fleac R, Racz G (2010) Experimental study on the surface quality of the medical implants obtained by single point incremental forming. Int J Mater Form 3(1):935–938. DOI: 10.1007/s12289-010-0922-x
3. Bagudanch I, Garcia-Romeu ML, Ferrer I, Ciurana J (2018) Customized cranial implant manufactured by incremental sheet forming using a biocompatible polymer. Rapid Prototyp J 24(1):120–129. DOI: 10.1108/RPJ-06-2016-0089
4. Piccininni A, Gagliardi F, Guglielmi P, Napoli LD, Ambrogio G, Sorgente D, Palumbo G, Saanouni K (2016) Biomedical Titanium alloy prostheses manufacturing by means of Superplastic and Incremental Forming processes. MATEC Web Conf 80:15007. DOI: 10.1051/matecconf/20168015007
5. Murugesan M, Dong WJ (2021) Formability and Failure Evaluation of AA3003-H18 Sheets in Single-Point Incremental Forming Process through the Design of Experiments. Materials 14(4):1–26. DOI: 10.3390/ma14040808

6. Cheng ZN, Li YL, Xu CX, Li FY (2020) Incremental sheet forming towards biomedical implants: a review. J Mater Res Technol 9(4):7225–7251. DOI: 10.1016/j.jmrt.2020.04.096
7. Hassan M, Hussain G, Wei H, Qadeer A, Alkahtani M (2021) Progress on single-point incremental forming of polymers. Int J Adv Manuf Technol 114(1–2):1–26. DOI: 10.1007/s00170-021-06620-7
8. Al-Ghamdi KA (2018) Spring back analysis in incremental forming of polypropylene sheet: An experimental study. J Mech Sci Technol 32(10):4859–4869. DOI: 10.1007/s12206-018-0934-x
9. Ambrogio G, Gagliardi F, Conte R, Russo P (2019) Feasibility analysis of hot incremental sheet forming process on thermoplastics. Int J Adv Manuf Technol 102(1–4):937–947. DOI: 10.1007/s00170-018-3180-6
10. Yang ZY, Chen F, Gatea S, Ou H (2020) Design of the novel hot incremental sheet forming experimental setup, characterization of formability behavior of polyether-ether-ketone (PEEK). Int J Adv Manuf Technol 106(11–12):5365–5381. DOI: 10.1007/s00170-020-05035-0
11. Lin J, Li J, Liu T, Zhu L, Guan Y (2020) Evaluation of friction reduction and frictionless stress in ultrasonic vibration forming process. J Mater Process Technol 288(7):116881. DOI: 10.1016/j.jmatprotec.2020.116881
12. Li YL, Wang ZJ, Zhai WD, Cheng ZN, Li FY, Li XQ (2021) The influence of ultrasonic vibration on parts properties during incremental sheet forming. Adv Manuf 9(2):250–261. DOI: 10.1007/s40436-021-00347-0
13. Li Y, Hu ZH, Liang JC, Liang C (2021) Research on Ultrasonic-Assisted Multi-Point Stretch Bending Process of Aluminum Profile. Int J Adv Manuf Technol 119(3–4):2259–2270. DOI: 10.1007/s00170-021-08408-1
14. Davarpanah MA, Bansal S, Malhotra R (2017) Influence of Single Point Incremental Forming on Mechanical Properties and Chain Orientation in Thermoplastic Polymers. J Manuf Sci Eng 139(2):021012. DOI: 10.1115/1.4034036
15. Hata K, Sakaguchi M, Kitamura R, Kobayashi S, Ogihar S (2019) Influence of molecular chain behavior on mechanical properties of poly-L-lactic acid by molecular dynamics method. Adv Compos Mater 28(629):1–13. DOI: 10.1080/09243046.2019.1618783
16. Wei HY, Hussain G, Heidarshenas B, Alkahtani M (2020) Post-Forming Mechanical Properties of a Polymer Sheet Processed by Incremental Sheet Forming: Insights into Effects of Plastic Strain, and Orientation and Size of Specimen. Polymers 12(9):E1870. DOI: 10.3390/polym12091870
17. Lu B, Li Z, Long H, Chen F, Chen J, Ou H (2017) Microstructure refinement by tool rotation-induced vibration in incremental sheet forming. Procedia Eng 207:795–800. DOI: 10.1016/j.proeng.2017.10.831
18. Sakhtemanian MR, Honarpisheh M, Amini S (2019) A novel material modeling technique in the single-point incremental forming assisted by the ultrasonic vibration of low carbon steel/commercially pure titanium bimetal sheet. Int J Adv Manuf Technol 102(1–4):473–486. DOI: 10.1007/s00170-018-3148-6

19. Liao J, Liu JH, Zhang LX, Xue X (2020) Influence of heating mode on orange peel patterns in warm incremental forming of magnesium alloy. Procedia Manuf 50:5–10. DOI: 10.1016/j.promfg.2020.08.002
20. Vanhove H, Verbert J, Gu J, Vasilakos I, Duflou JR (2010) An experimental study of twist phenomena in single point incremental forming. Int J Mater Form 3(1):975–978. DOI: 10.1007/s12289-010-0932-8
21. Tao G, Chen YM, Mu JS, Zhang LT, Ye CL, Li W (2021) Exploring the entangled state and molecular weight of UHMWPE on the microstructure and mechanical properties of HDPE/UHMWPE blends. J Appl Polym Sci 138(30):1097–4628. DOI: 10.1002/app.50741
22. Yang YQ, Duan HJ, Zhang G, Long SR, Yang J, Wang XJ (2013) Effect of the contribution of crystalline and amorphous phase on tensile behavior of poly (phenylene sulfide). Polym Res 20(7):1022–9760. DOI: 10.1007/s10965-013-0198-1
23. Yang LY, Su JQ, Yang Q, Zhang TY, Zhao ZG, Huang YJ, Liao X (2016) Effective in situ polyamide 6 microfibrils in isotactic polypropylene under microinjection molding: significant improvement of mechanical performance. J Mater Sci 51(23):10386–10399. DOI: 10.1007/s10853-016-0259-z
24. Sinha AK, Narang HK, Bhattacharya S (2020) Mechanical properties of hybrid polymer composites: a review. J Braz Soc Mech Sci Eng 42(8):1–13. DOI: 10.1007/s40430-020-02517-w
25. Lozano-Sánchez LM, Bagudanch I, Sustaita AO, Iturbe-Ek J, Elizalde LE, Garcia-Romeu ML, Elías-Zúñiga A (2018) Single-Point Incremental Forming of Two Biocompatible Polymers: An Insight into Their Thermal and Structural Properties. Polymers 10(4):391. DOI: 10.3390/polym10040391
26. Yang MS, Bai L, Li Y, Yuan QL, Ferro P (2019) Influences of Vibration Parameters on Formability of 1060 Aluminum Sheet Processed by Ultrasonic Vibration-Assisted Single Point Incremental Forming. Adv Mater Sci Eng 2019:1–12. DOI: 10.1155/2019/8405438
27. Langford JI, Wilson A (2015) Scherrer after sixty years: A survey and some new results in the determination of crystallite size. J Appl Crystallogr 11(7):102–113. DOI: 10.1063/1.4928401
28. Tomisawa R, Oneda S, Ikaga T, Kim K, Ohkoshi Y, Okada K, Masunaga H, Kanaya T, Katsuta H, Funatsu Y (2019) Effects of dimensions and regularity on the mechanical properties of the smectic phase formed during orientation-induced crystallization of poly(ethylene terephthalate). Polymer 164:163–173. DOI: 10.1016/j.polymer.2019.01.002
29. Liu Q, Sun X, Li H, Yan S (2013) Orientation-induced crystallization of isotactic polypropylene. Polymer 54(17):4404–4421. DOI: 10.1016/j.polymer.2013.04.066

Figures

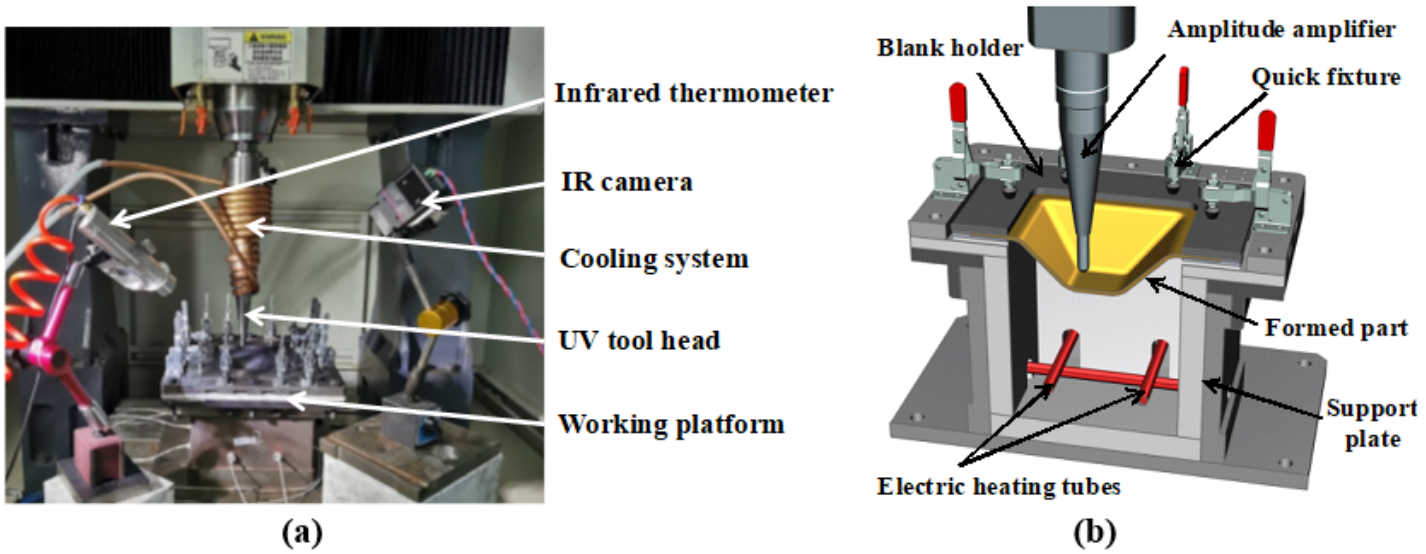

Figure 1

(a) Experimental setup for UV-assisted thermal SPIF ; (b) Sectional view of working platform.

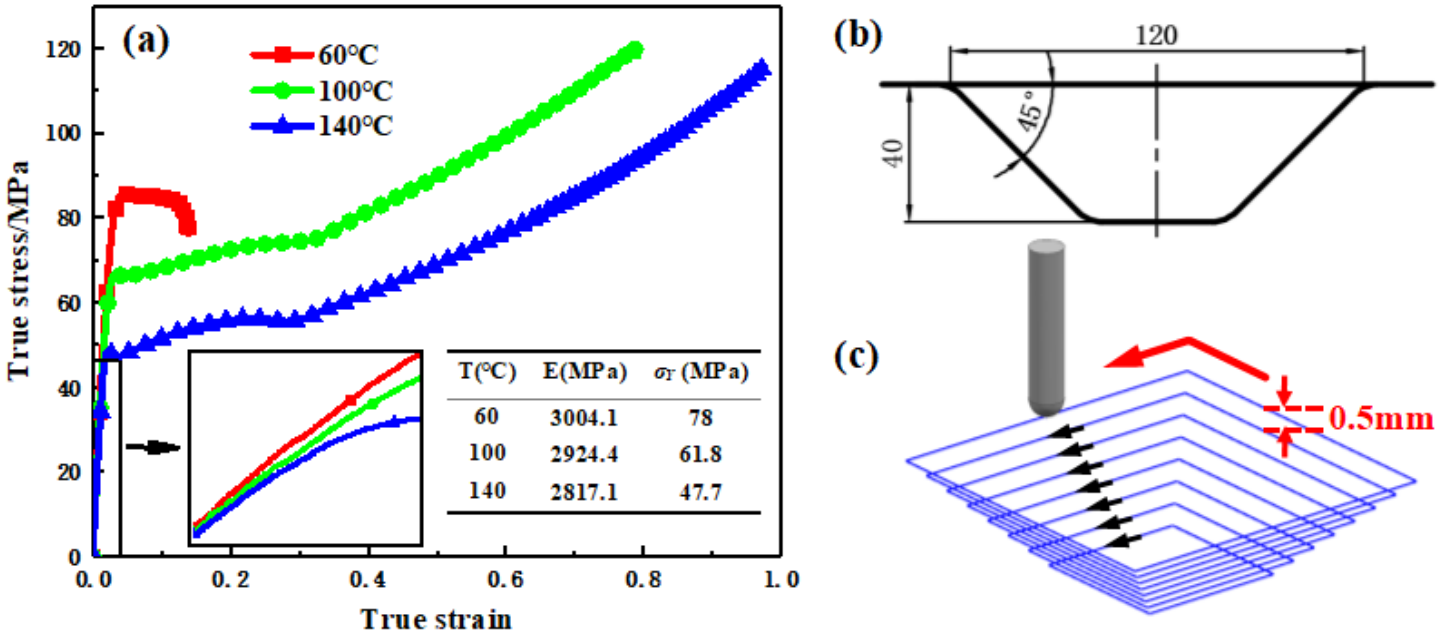

Figure 2

(a) Stress-Strain curves of PEEK at different temperatures; (b) The square pyramid with consistent wall angle; (c) Tool trajectory.

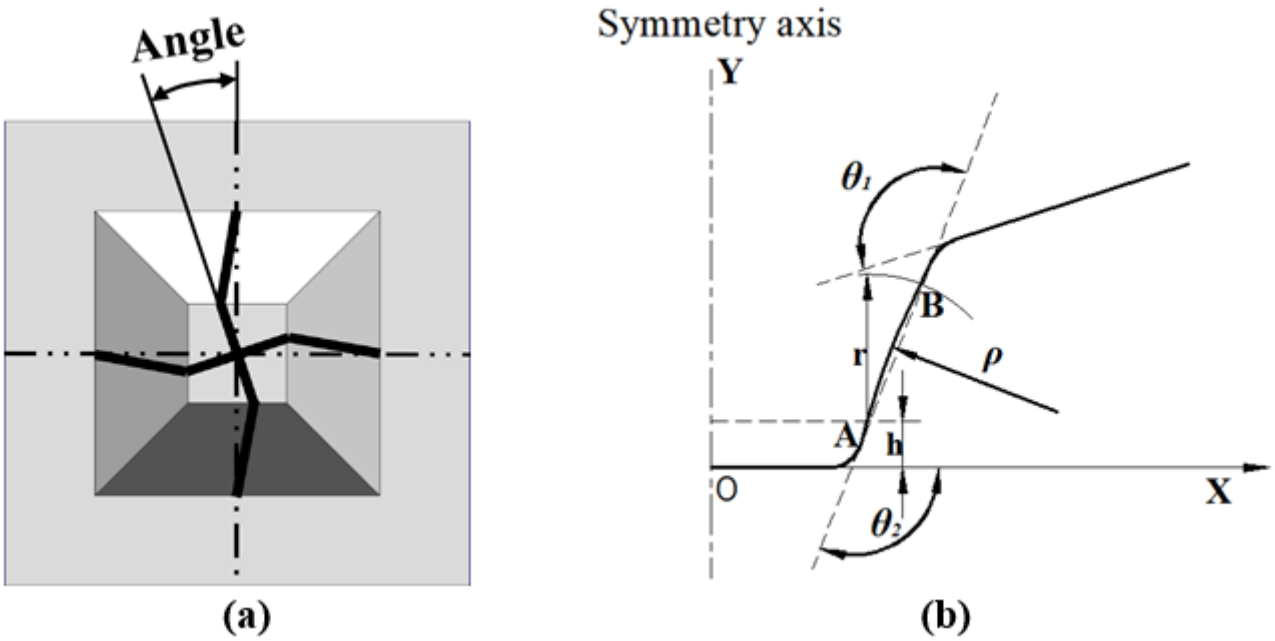

Figure 3

Measurement of (a) twist angle φ, (b) springback angle θ_1 , θ_2 and sidewall curl radius ρ.

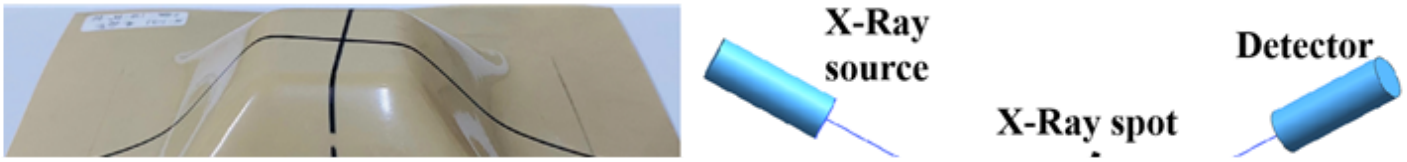

Figure 4

Schematic of XRD analysis.

Figure 5

Parts formed under different parameters.

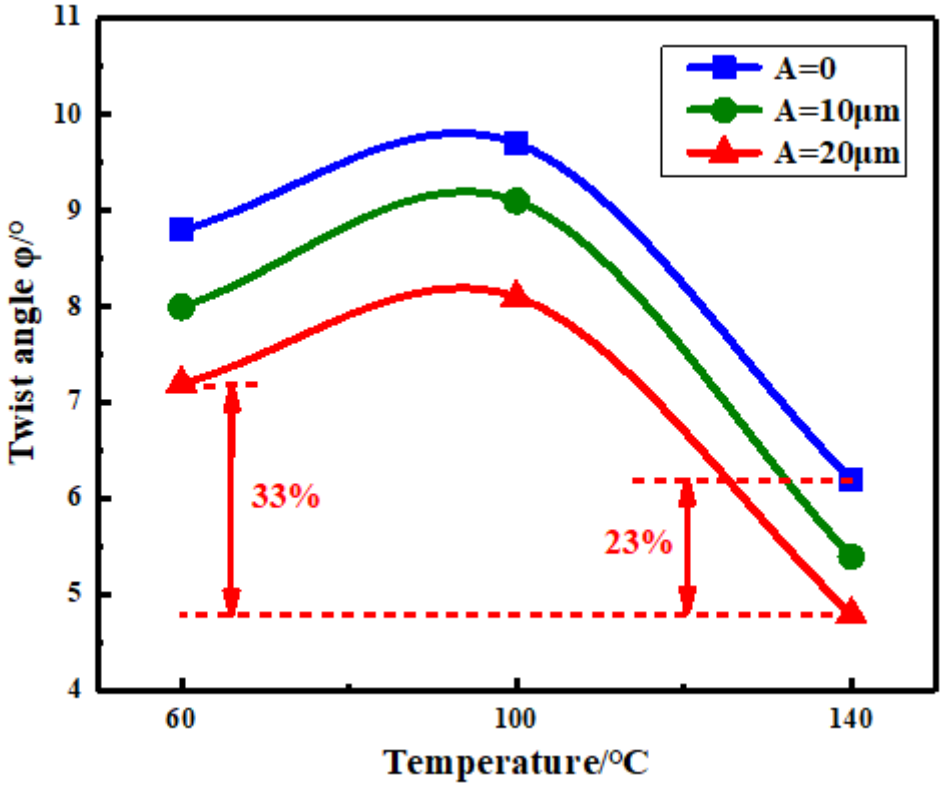

Figure 6

The twist angle φ of PEEK parts

Figure 7

(a) The inner surface of PEEK part, the scratches at (b) 60 °C, (c) 100 °C and (d) 140 °C.

Figure 8

Comparison of (a) springback angles θ_1, θ_2 and (b) curl radius ρ of side wall.

Figure 9

Thickness distribution of PEEK formed parts for (a) T=60 ℃, (b) T=100 ℃, (c) T=140 ℃ at different amplitudes; (d) Maximum thinning rate of PEEK formed parts.

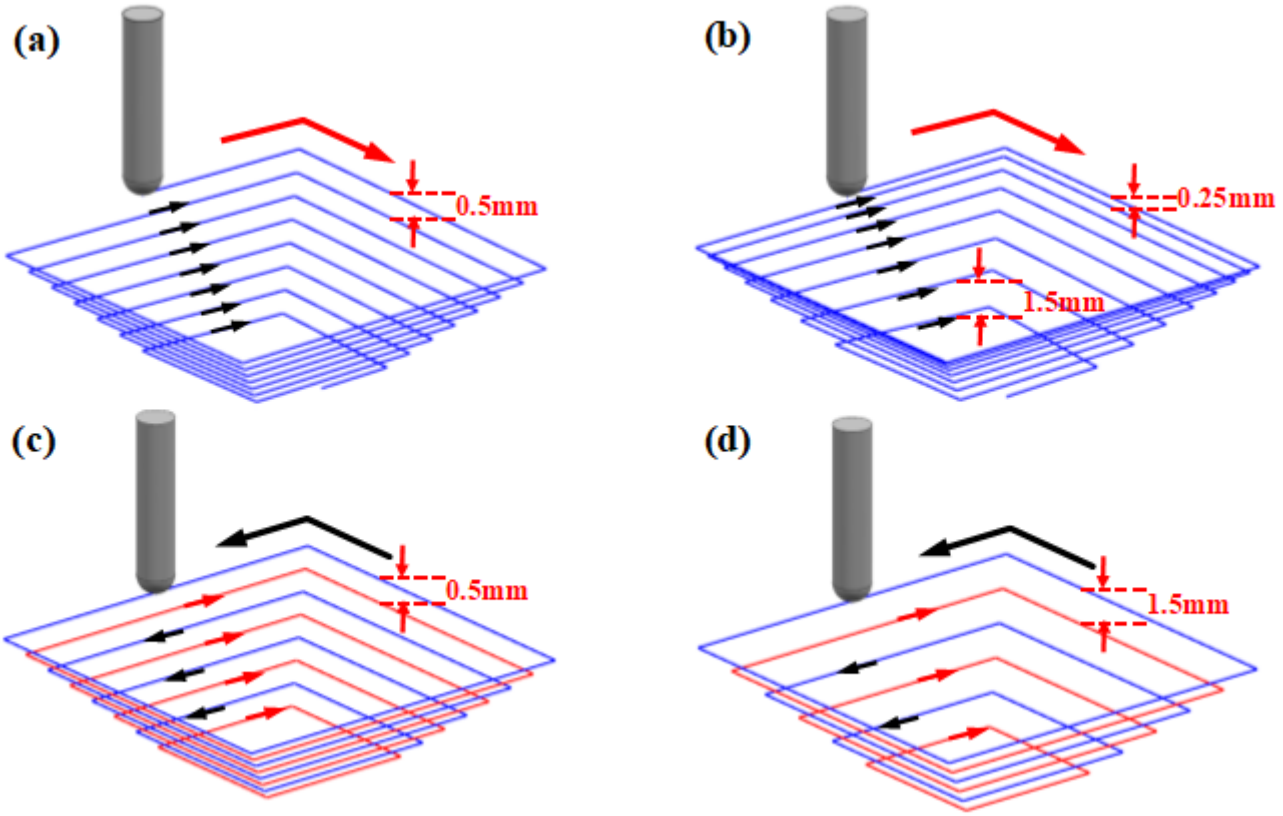

Figure 10

Schematics of different trajectories: (a) EST, (b) NEST, (c) MCT-0.5, (d) MCT-1.5.

Figure 11

The twist angle φ under different trajectories.

Figure 12

(a) section view of formed parts under different trajectories, (b) forming height and error of PEEK parts.

Figure 13

Comparison of (a) springback angles θ_1, θ_2 and (b) curl radius ρ of side wall under different trajectories.

Figure 14

XRD pattern of PEEK unformed sample.

Figure 15

XRD patterns of PEEK formed parts at different temperatures.

Figure 16

XRD patterns of PEEK formed parts for (a) T=60 ℃, (b) T=100 ℃, (c) T=140 ℃ at different amplitudes.

Figure 17

(a) Crystallinity and (b) crystallite size of formed and unformed PEEK parts.